Biosensors and Bioelectronics 142 (2019) 111579

Contents lists available at ScienceDirect

Biosensors and Bioelectronics

journal homepage: www.elsevier.com/locate/bios

A photoelectrochemical biosensor based on fullerene with methylene blue as a sensitizer for ultrasensitive DNA detection

Dan Long, Mengjie Li, Haihua Wang, Haijun Wang, Yaqin Chai**, Ruo Yuan*

Key Laboratory of Luminescent and Real-Time Analytical Chemistry (Southwest University), Ministry of Education, College of Chemistry and Chemical Engineering, Southwest University, Chongqing, 400715, PR China

ARTICLE INFO

Keywords:
Photoelectrochemical biosensor
DNA detection
Fullerene
Methylene blue
Sensitizer

ABSTRACT

In this protocol, a photoelectrochemical (PEC) biosensor based on methylene blue (MB) sensitized fullerene (C_{60}) was designed for ultrasensitive DNA detection. First, C_{60} nanoparticles (C_{60} NPs) as photoactive material was modified on the electrode surface to obtain an initial photocurrent signal. Additionally, the nicking endonuclease (Nb.BvCI enzyme)-assisted signal amplification strategy was implemented to transform limited target to plenty of products, which hybridized with DNA2 to form plentiful DNA duplex for immobilizing numerous MB as the sensitizer, thus accomplishing the effective sensitization toward C_{60} NPs and achieving an enhanced photocurrent for quantitatively detecting target DNA. This established PEC strategy realized the target DNA detection with the detection limit down to 3.3 fM, which paved a new avenue for DNA determination and exhibited huge application potential for other biomarkers in clinical analysis and disease diagnosis.

1. Introduction

Tuberculosis (TB) is one of the most fatal infectious diseases and remains one of the main reasons of mortality, causing more than 2 million deaths every year (Golichenari et al., 2018; Li et al., 2014). It is extremely difficult to prevent and control TB mainly because it could travel through the air and spread widely and rapidly especially in densely populated urban areas, posing a serious threat to public health and causing enormous economic losses to society (Barroso et al., 2018; Jing et al., 2014). As the pathogenic agent of TB, mycobacterium tuberculosis (MTB) causes the highest mortality rates than any other bacterial pathogen around the world, which could be employed as an effective biomarker for early diagnosis of TB (Faddoul, 2015; Mi et al., 2012). Therefore, sensitive and rapid detection of the specific DNA fragment (a fragment sequence of MTB) can supply important information for the diagnosis and treatment of TB. Although varieties of analysis methods, including electrochemiluminescence (Li et al., 2014), colorimetry (Teengam et al., 2017), and electrochemistry (Sypabekova et al., 2019), have been conducted for DNA detection and exhibited excellent analytical performance, the stability and sensitivity of these techniques ought to be enhanced further for meeting the requirement of ultrasensitive DNA detection. The photoelectrochemical (PEC) assay, a vibrantly developing analytical technique, possesses its outstanding merits, such as low background signal, simple operation, low cost and high sensitivity (Fan et al., 2016; Li et al., 2019; Kong et al., 2018; Zhang et al., 2018; Zhao et al., 2014, 2018), which has aroused intense research interest in the detection of various analytes (Hou et al., 2018; Wang et al., 2013). As yet, utilizing PEC technique for the estimation of the specific DNA fragment (a fragment sequence of MTB) has rarely been reported. Thus, there is a desirable need to design a PEC biosensor for detecting the DNA fragment of MTB rapidly and sensitively.

Recently, fullerene (C_{60}) as a prominent photoelectric material has attracted widespread concern in the field of PEC sensing as a result from its inherent characteristics. For instance, in the entire UV-visible (UV-vis) spectrum, it has obvious electronic absorption bands (Bonifazi et al., 2007; Hu et al., 2013). Besides, it also has strong electron-accepting capacity (Lian et al., 2015; Wang et al., 2018a). Nevertheless, the photoelectric conversion efficiency and wider application were restricted (Kim et al., 2015; Wang et al., 2018a) by its wide band gap (Li et al., 2017). For pursuing an improved photocurrent response, sensitization strategy is a feasible approach to conquer the above problem (Wang et al., 2018a). Until now, a great deal of effort has been made for an enhanced PEC function of C_{60} by using some sensitizers. For instance, Hu's group utilized a signal probe made of carbon nanotube – Congo red – C_{60} nanohybrids to establish a PEC immunosensor for ultrasensitive carcinoembryonic antigen determination (Hu et al., 2013). Lately, our group proposed a PEC aptasensor for ultrasensitive thrombin detection relying upon fullerene/CdTe quantum dots

* Corresponding author.
** Corresponding author.
E-mail addresses: yqchai@swu.edu.cn (Y. Chai), yuanruo@swu.edu.cn (R. Yuan).

https://doi.org/10.1016/j.bios.2019.111579
Received 16 July 2019; Received in revised form 5 August 2019; Accepted 8 August 2019
Available online 09 August 2019
0956-5663/

sensitized structure (Li et al., 2016). Although the enhanced photoelectric conversion efficiency of C_{60} has been achieved by these strategies, some disadvantages including limited immobilization, time-consuming preparation, and high toxicity still existed. Accordingly, it is necessary to seek for a sensitizer with high immobilization efficiency, easy preparation, low toxicity and outstanding sensitization effect for constructing C_{60} − based PEC sensing. Recently, several dyes (Wu et al., 2014; Yan et al., 2016; Zhao et al., 2015) with stable physicochemical properties and strong light absorption capacity have been used as sensitizers for improving the photocurrent conversion efficiency. Among a variety of dyes, methylene blue (MB) is an organic small molecular dye with low toxicity, which can accelerate electron transfer throughout the helix structure and strengthen the conductivity of DNA (Gill et al., 2005). Recent years, it has been reported that MB could be easily embedded in DNA duplex as a redox-active intercalator (Da et al., 2018; Li et al., 2018; Zhou et al., 2013). Considering the inherent merits of MB, in this work, we utilized MB embedded in the DNA duplex as a sensitizer of C_{60} NPs to improve its photoelectric conversion efficiency.

Herein, a PEC biosensor was proposed for ultrasensitive detection of target DNA (a DNA fragment of MTB) *via* employing C_{60} NPs as photoactive material and MB as sensitizer, which was depicted in Scheme 1. Firstly, C_{60} NPs and Au nanoparticles layer were sequentially modified to the electrode surface. Next, DNA2 which was used to hybridize with product to form DNA duplex for immobilizing numerous MB was immobilized onto the resulted electrode surface *via* Au–S bonds. After that, hexanethiol (HT) was coated onto the surface of the electrode for blocking the nonspecific binding sites. Additionally, after DNA walker (DW) was released from the duplex of DW and protection DNA (PD), it could hybridize with DNA1 which has the specific cleavage site of the nicking endonuclease (Nb.BvCI enzyme). After that, the Nb.BvCI enzyme conducted the specific cleavage toward DNA1, thus producing plenty of products. Then, the obtained electrode was incubated with products so that DNA2 could hybridize with products to form DNA duplex. Subsequently, plenty of MB could be inset into the DNA duplex, realizing effective sensitization for C_{60} NPs, thus attaining a dramatically increased photocurrent signal for quantitatively estimating target. Significantly, the elaborated biosensor accomplished sensitive and specific photoelectrochemical DNA detection, which opened a new way for TB diagnosis in clinical analysis.

2. Experimental section

2.1. Synthesis of Fe_3O_4@Au, C_{60} NPs, and MB solution

Fe_3O_4@Au was synthesized according to our reported work (Xie et al., 2016). C_{60} NPs was prepared as our previous method with a slight modification (Li et al., 2016). Firstly, 2 mg fullerene was put into 2 mL toluene followed by ultrasonication until homogeneous purple solution

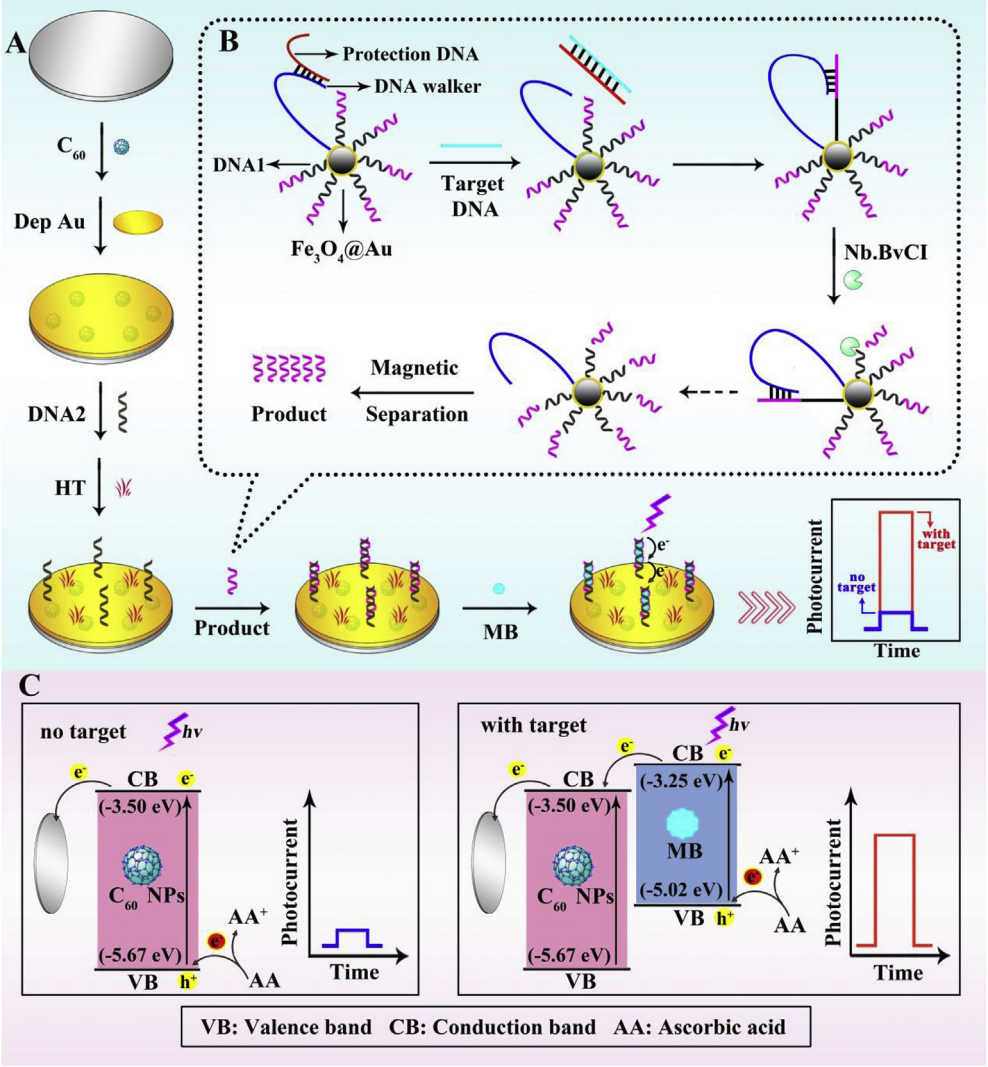

Scheme 1. The construction procedure of the PEC biosensor based on fullerene with methylene blue as a sensitizer for ultrasensitive DNA detection (A), the detailed enzyme-assisted signal amplification procedure (B), and the mechanism for photocurrent generation (C).

obtained. Secondly, 2 mL ultrapure water was added to it with ultrasonication for two days. Lastly, the attained C_{60} NPs solution was kept at 4 °C. For MB solution preparation, 0.0112 g MB powder was dispersed into 10 mL PBS solution (pH 7.0) to achieve uniform blue solution. The prepared MB solution was stored at 4 °C.

2.2. The Nb.BvCI enzyme-assisted signal amplification

Scheme 1B showed the enzyme-assisted signal amplification strategy schematically. Briefly, 100 μL 2.5 μM DNA walker (DW) and 100 μL 2.5 μM protection DNA (PD) were mixed and reacted for 2 h at 37 °C to complete the hybridization. Next, the resulted solution was mixed with 500 μL Fe_3O_4@Au and 100 μL 6.25 μM DNA1 and then stirred at 4 °C for 12 h. Thus DNA1 and DW could be immobilized on the Fe_3O_4@Au surface *via* Au–S bonds. Subsequently, the above mixture was centrifuged at 12000 rpm for 5 min for removing unreacted reagents and then dispersed in 400 μL PBS solution (pH 7.0). Then, the mixture reacted with 100 μL target DNA at 37 °C for 10 min so that target could hybridize with PD to release DW. After that, DW could hybridize with DNA1. Finally, the obtained solution was incubated with 2 μL nicking endonuclease (20 U) and 4 μL 10 × NE Buffer at 37 °C for 1 h. As a result, the partial bases from the 3′-end to the specific cleavage site of DNA1 (5′-▼TGAGGATATCG-3′) could be specifically cleaved by the enzyme, generating abundant products. Finally, PEC measurements were conducted by dropping the supernatant attained by magnetic separation onto the modified electrode.

2.3. Construction of the PEC biosensor

Scheme 1A displayed the detailed fabrication steps of the PEC biosensor. Prior to modification, 0.3 μm and 0.05 μm alumina powder were utilized for polishing the bare GCE followed by ultrasonically washing with ethanol and ultrapure water to attain a mirror-like surface. Firstly, the preprocessed electrode was coated with 10 μL C_{60} NPs and then dried for 20 min at 37 °C to get a homogeneous film. Next, in 1% $HAuCl_4$ solution, an Au nanoparticles (Au NPs) layer was deposited on the surface of the modified electrode (Dep Au) at − 0.2 V for 30 s. Subsequently, 15 μL 2 μM DNA2 was immobilized on the surface of the electrode *via* Au–S bonds at 4 °C for 12 h. After that, to block the nonspecific binding sites, the modified electrode was incubated with 10 μL 1 mM HT for 30 min at room temperature. Then, 15 μL product was incubated on the modified electrode for 2 h at 37 °C so that product could hybridize with DNA2 to form DNA duplex. Finally, 20 μL MB was incubated on the resulted electrode for 1 h at 37 °C. Hence, MB could be embedded into the duplex of DNA2 and product. Physically absorbed species were removed by ultrapure water with carefully wash after each step.

3. Results and discussions

3.1. Characterization of the synthesized materials

Transmission electron microscopy (TEM) was utilized to characterize the morphology of the prepared C_{60} NPs. As illustrated in Fig. 1A, the synthesized C_{60} NPs possessed globular structure with the size about 20 nm, suggesting that C_{60} NPs was successfully prepared. The insert of Fig. 1A was the TEM magnification scale of C_{60} NPs. In Fig. 1B, scanning electron microscopy (SEM) was carried out to characterize the morphology and size of Fe_3O_4@Au. Fe_3O_4@Au had globular structure with the size about 250 nm and numerous Au NPs were attached tightly on the surface of the amido-modified Fe_3O_4 (Fe_3O_4–NH_2) magnetic microspheres, which indicated that Fe_3O_4@Au was synthesized successfully. In Fig. 1D, TEM elemental mapping images were employed to further verify the successful synthesis of Fe_3O_4@Au. Curve (b-d) and (f-i) showed the elements of Fe, O, and N in the Fe_3O_4–NH_2 magnetic microspheres and Fe, O, N, and Au in the Fe_3O_4@Au, respectively. The above results also verified that Fe_3O_4@Au was prepared successfully. Besides, the successful preparation of MB solution was examined by UV-vis absorption spectroscopy. As illustrated in Fig. 1C, C_{60} NPs (curve a) showed three absorption peaks at 266, 345, and 455 nm, respectively. Besides, MB solution (curve b) possessed four characteristic absorption peaks at 245, 291, 616, and 663 nm, respectively, which was consistent with the reported work (Schafer et al., 2013).

3.2. Investigation of the optical band gap (E_g), valence band, and conduction band for the photoactive materials

Optical and electrochemical measurements were conducted to evaluate the energy levels of C_{60} NPs and MB. Ferrocene was regarded as the reference substrate with an assumed vacuum level of 4.8 eV and the onset oxidation position of 0.48 V (Wang et al., 2018b). The E_g and E_{VB} were estimated according to the onset absorption wavelength (λ_{onset}) in the UV − vis absorption spectrum and the onset oxidation peak in the CV curve, respectively, which was according to the following formula:

$$E_g = 1240 / \lambda_{onset}$$

$$E_{VB} = -(4.8 + E_{oxidation} - E_{1/2(reference)})$$

$$E_{CB} = E_{VB} + E_g$$

In Fig. 2A, the λ_{onset} of C_{60} NPs and MB were 571 and 700 nm, respectively, so corresponding E_g were estimated to 2.17 eV and 1.77 eV. In Fig. 2B, the onset oxidation position of C_{60} NPs and MB showed 1.35 V (E_a) and 0.70 V(E_b), so corresponding E_{VB} of C_{60} NPs and MB were calculated to − 5.67 eV and − 5.02 eV, respectively. Consequently, E_{CB} of C_{60} NPs and MB were determined to − 3.50 eV and − 3.25 eV, respectively.

3.3. The sensitized mechanism of the photoelectric material

A PEC biosensor depending upon C_{60} NPs/MB sensitized structure was established for sensitively determining DNA in this protocol. As an eminent photoelectric material, C_{60} NPs possessed outstanding merits. For instance, in the entire UV-vis spectrum, it has obvious electronic absorption bands (Bonifazi et al., 2007; Hu et al., 2013). Furthermore, it has strong electron-accepting capacity (Lian et al., 2015; Wang et al., 2018a). Unfortunately, limited photocurrent conversion efficiency resulted from the wide band gap (Wang et al., 2018a). In this respect, by combining narrow band gap material with wide band gap C_{60} NPs, the utilization of light energy and charge separation were facilitated and the electron-hole recombination was reduced, resulting in evidently enhanced PEC signal (Zhao et al., 2015). Compared with C_{60} NPs, MB has narrower band gap (1.77 eV) that was calculated according to the reported work (Wang et al., 2018b). The photoelectric conversion efficiency was improved by the narrow band gap of MB that benefited injection of photogenerated electrons from MB to C_{60} NPs. The photocurrent generation mechanism of the C_{60} NPs/MB sensitized platform was illustrated in Scheme 1C. Briefly, electrons of MB transferred from valence band (VB) to conduction band (CB), producing a series of electron-hole pairs under excitation light source at 460 nm. Afterwards, the photoexcited electrons migrated to the CBs of C_{60} NPs and then moved to the bare GCE surface, thus generating a strong photocurrent signal. Simultaneously, AA was used as electrons donor to promote charge separation as well as restrain the recombination of electron-hole pairs, thus obtaining an improved and continuous photocurrent signal.

3.4. Electrochemical characterization of the constructed biosensor

To verify the successful fabrication of the PEC biosensor, CV and EIS were employed to characterize the construction procedure. As

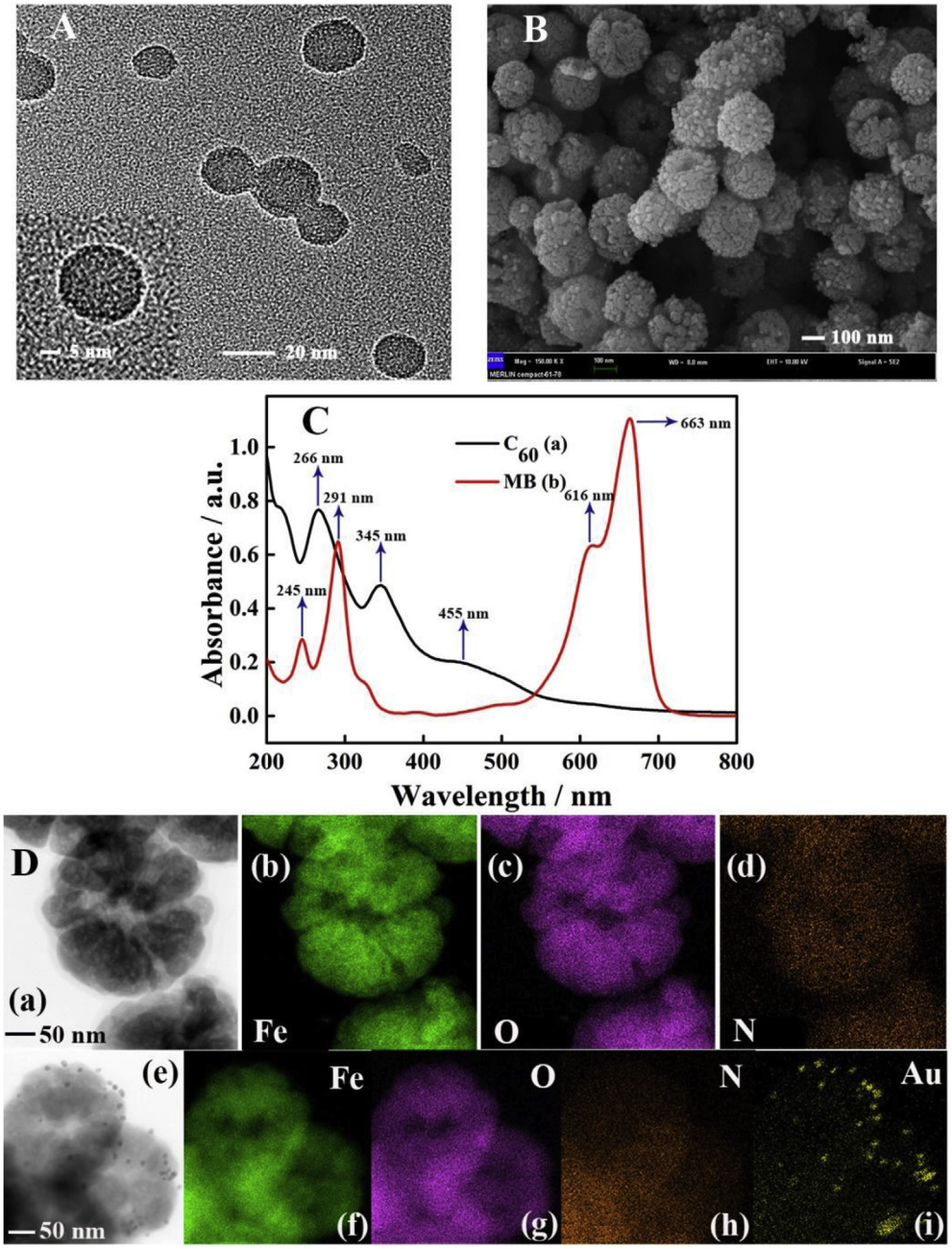

Fig. 1. (A) TEM image of C_{60} NPs. The insert of (A) was the TEM magnification scale of C_{60} NPs; (B) SEM image of Fe_3O_4@Au; (C) The UV-vis adsorption spectrums of C_{60} NPs (a) and MB (b); (D) TEM and elemental mapping images of Fe_3O_4–NH_2 (a–d) and Fe_3O_4@Au (e–i).

displayed in Fig. 3A, a pair of beautiful redox peak current was achieved by the pretreated bare GCE (curve a). The peak current sharply decreased with C_{60} NPs coated onto bare GCE (curve b), because the transmission of electrons could be hampered by C_{60} NPs. After the step of Dep Au, the peak current enhanced dramatically because Au NPs has excellent conductivity (curve c). Curve d, e, and f respectively exhibited consecutive decrease when DNA2, HT and product were successively immobilized on the modified electrode because of the increased electronic repulsion and steric hindrance effect. Lastly, the peak current (curve g) showed a moderate increase when MB was incubated on the resulted electrode, which was mainly attributed to the effective sensitization of MB towards C_{60} NPs. Meanwhile, EIS measurement was also carried out to investigate the stepwise construction procedure. As shown in Fig. 3B, compared with the bare GCE (curve a), the charge-transfer resistance (R_{et}) sharply increased (curve b) with C_{60} NPs coated onto the GCE surface, which could be attributed to that the electron transfer could be hampered by the homogeneous film of C_{60} NPs. After the step of Dep Au, the R_{et} decreased (curve c) because the Au NPs possessed excellent conductivity. After the stepwise assembling of DNA2, HT and product, the R_{et} increased consecutively (curve d, e and f, respectively). When MB was immobilized on the modified electrode surface, a remarkable decrease of the R_{et} was observed (curve g), because the massive MB inserted into the DNA duplex exhibited superior conductivity. The results suggested that this PEC sensing interface was constructed successfully.

3.5. PEC characterization of the biosensor

The stepwise-constructed process of the established PEC biosensor was examined by the photocurrent characterization toward 1 nM target

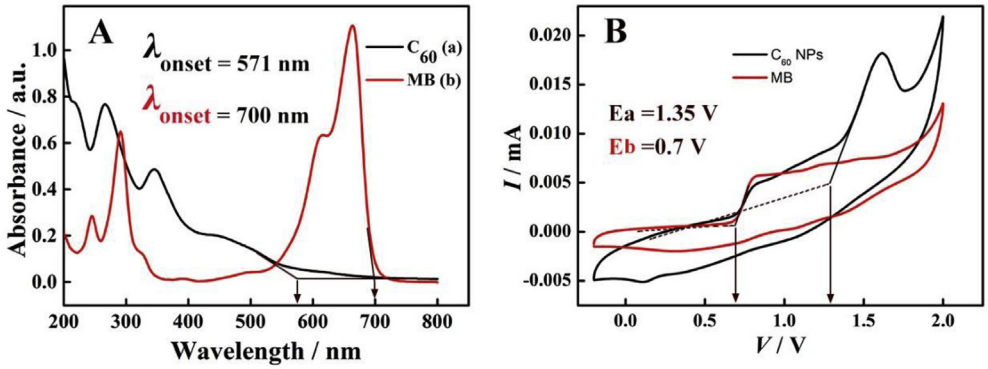

Fig. 2. (A) The UV-vis adsorption spectrums of C_{60} NPs (a) and MB (b); (B) The CV measurements of the bare GCE modified by C_{60} NPs and MB in a deoxygenated anhydrous acetonitrile solution (5 mL) containing 0.1 M tetrabutylammonium hexafluorophosphate at 50 mV/s.

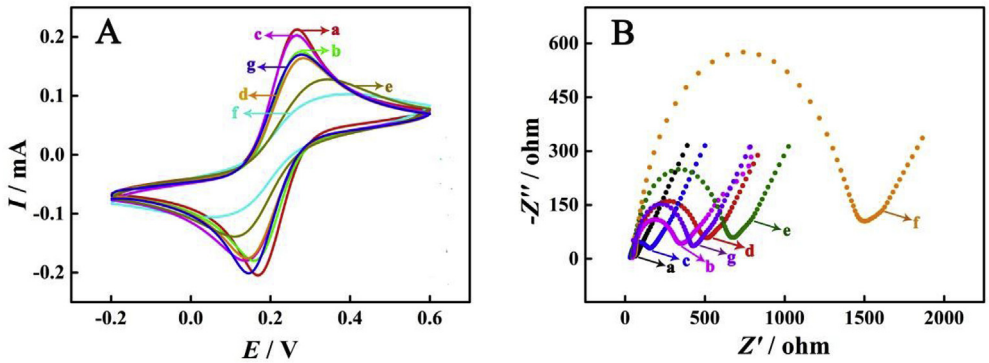

Fig. 3. CV and EIS responses of bare GCE (a), C_{60} NPs/GCE (b), Dep Au/C_{60} NPs/GCE (c), DNA2/Dep Au/C_{60} NPs/GCE (d), HT/DNA2/Dep Au/C_{60} NPs/GCE (e), product/HT/DNA2/Dep Au/C_{60} NPs/GCE (f) and MB/product/HT/DNA2/Dep Au/C_{60} NPs/GCE (g).

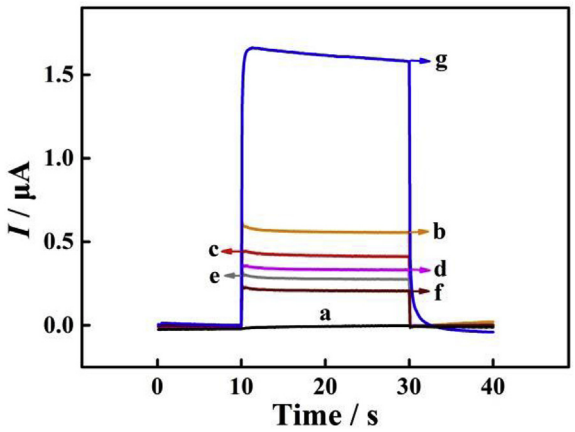

Fig. 4. PEC responses toward 1 nM target DNA of bare GCE (a), C_{60} NPs/GCE (b), Dep Au/C_{60} NPs /GCE (c), DNA2/Dep Au/C_{60} NPs/GCE (d), HT/DNA2/Dep Au/C_{60} NPs/GCE (e), product/HT/DNA2/Dep Au/C_{60} NPs/GCE (f) and MB/product/HT/DNA2/Dep Au/C_{60} NPs/GCE (g).

DNA. As shown in Fig. 4, the bare GCE showed a photocurrent (curve a) near zero. After C_{60} NPs was dropped on the preprocessed bare GCE, the photocurrent (curve b) increased remarkably, which was attributed to that C_{60} NPs has excellent photoelectric activity. After immobilization of Au NPs, the photocurrent (curve c) decreased for the negatively charged Au NPs excluded the negative charged AA to the electrode surface (Cui et al., 2018). After the stepwise assembling of DNA2, HT and product, the photocurrent declined consecutively (curve d, e and f, respectively) because both DNA skeleton and small organic molecules have poor charge transfer. Finally, when MB was incubated on the modified electrode, a conspicuous increase of photocurrent (curve g) was obtained, since numerous MB inset into DNA duplex could achieve the effective sensitization to C_{60} NPs.

3.6. Analytical performance of developed biosensor

The analytical performance of this proposed PEC biosensor was investigated by measuring the photocurrent subject to various concentrations of target DNA. Fig. 5A showed that the photocurrent signal increased linearly with target concentration increasing from 10 fM to 100 nM. Moreover, the limit of detection was estimated as 3.3 fM on the basis of the 3σ rule. The linear equation was $I = 0.1512 \lg c + 1.094$ ($R^2 = 0.9962$, where I and c were the photocurrent signal and the target concentration, respectively). And the added error bar implied the detection standard deviation (n = 10). Additionally, compared with the methods reported previously, this assay showed a superior sensitivity and a wider linear range for DNA detection (Table S3), which proved that this elaborated PEC biosensor embraced extraordinary potential for ultrasensitive DNA determination.

3.7. Selectivity and stability of the PEC biosensor

Herein, to investigate the selectivity of this proposed biosensor, several possible interfering substances were utilized in control experiments. As illustrated in Fig. 6A, the control experiments were carried out *via* employing smDNA (100 pM), dmDNA (100 pM), tmDNA (100 pM) and the mixture sequences to replace target DNA (1 pM), respectively. Consequently, the photocurrent responses of smDNA, dmDNA, and tmDNA showed negligible change compared to the blank, and the added error bar implied the detection standard deviation (n = 3). On the contrary, a remarkable increase of the photocurrent intensity of the target DNA and the mixture sequences could be observed, suggesting that the developed PEC biosensor showed brilliant selectivity for target

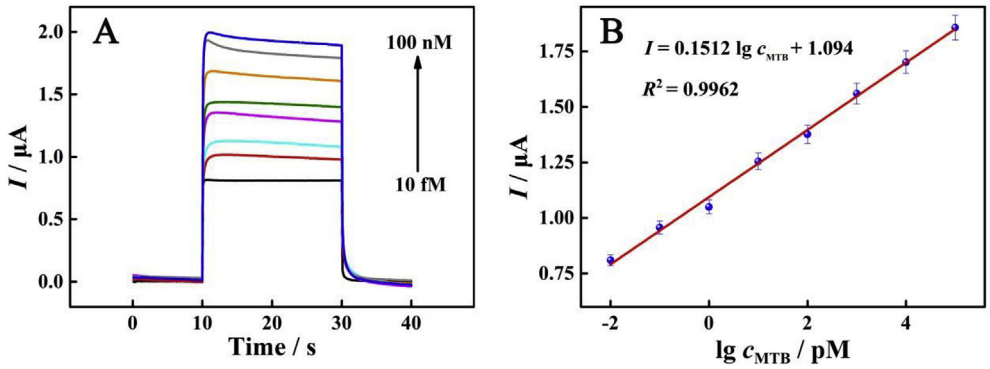

Fig. 5. PEC signals of the biosensor with various concentrations: 10.0 fM, 100 fM, 1.00 pM, 10.0 pM, 100 pM, 1.00 nM, 10.0 nM and 100 nM (A). Working curve between the photocurrent and the logarithm of different DNA concentration (B).

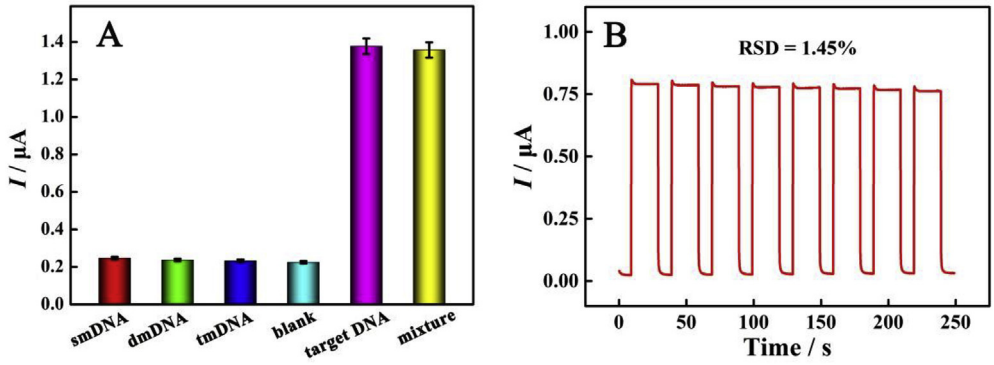

Fig. 6. (A) The study of selectivity for the PEC biosensor by using different interferences (smDNA, dmDNA, tmDNA, and mixture) to replace target DNA and (B) stability of the PEC biosensor incubated with 10 fM target.

DNA detection. Besides, the proposed PEC biosensor exhibited a desirable stability with 10 fM target under periodic off-on-off light for 8 cycles. Fig. 6B showed the relative standard deviation (RSD) of 1.45% for photocurrent signal, which implied a superb stability of the constructed PEC biosensor.

4. Conclusions

In conclusion, we proposed a novel PEC biosensor for ultrasensitive detection of DNA on the basis of MB as sensitizer for sensitizing C_{60} NPs coupling with the Nb.BvCI enzyme-assisted signal amplification strategy. The C_{60} NPs/MB sensitized structure exhibited nearly 3.5-fold high PEC signal compared with separate C_{60} NPs on account of the effective sensitization of MB toward C_{60} NPs. Moreover, the introduction of the enzyme-assisted signal amplification strategy could improve the detection sensitivity of this biosensor. As a consequence, the established PEC strategy with superior selectivity and stability is expected to be an alternative and low-cost tool for detecting DNA and opens a new avenue for sensitive determination of other biomarkers in disease diagnosis. However, the sensitivity and detection limit remained unsatisfactory compared with some literatures employing PEC method for DNA detection (Wang et al., 2018a, 2019). In the future, we will pay much attention to photoactive materials with superior performance and amplification of target DNA with higher efficiency.

CRediT authorship contribution statement

Dan Long: Conceptualization, Data curation, Formal analysis, Investigation, Writing - original draft, Writing - review & editing. **Mengjie Li:** Data curation, Investigation. **Haihua Wang:** Conceptualization, Writing - original draft, Supervision. **Haijun Wang:** Conceptualization, Writing - original draft, Supervision. **Yaqin Chai:** Funding acquisition, Resources, Project administration, Supervision. **Ruo Yuan:** Funding acquisition, Resources, Writing - review & editing.

Declaration of competing interest

The authors declare that they have no known competing financial interests or personal relationships that could have appeared to influence the work reported in this paper.

Acknowledgements

This work was financially supported by the National Natural Science Foundation of China (21575116, 21775124, 21675129) and the Fundamental Research Funds for the Central Universities (XDJK2018AA003), China.

Appendix A. Supplementary data

Supplementary data to this article can be found online at https://doi.org/10.1016/j.bios.2019.111579.

References

Barroso, T.G., Martins, R.C., Fernandes, E., Cardoso, S., Rivas, J., Freitas, P.P., 2018. Biosens. Bioelectron. 100, 259–265.
Bonifazi, D., Enger, O., Diederich, F., 2007. Chem. Soc. Rev. 36, 390–414.
Cui, L., Hu, J., Wang, M., Diao, X.K., Li, C.C., Zhang, C.Y., 2018. Anal. Chem. 90, 11478–11485.
Da, H.M., Liu, H.Y., Zheng, Y.N., Yuan, R., Chai, Y.Q., 2018. Biosens. Bioelectron. 101, 213–218.
Faddoul, D., 2015. Adv. Pediatr. 62 (1), 59–90.
Fan, G.C., Shi, X.M., Zhang, J.R., Zhu, J.J., 2016. Anal. Chem. 88, 10352–10356.
Gill, R., Patolsky, F., Katz, E., Willner, I., 2005. Angew. Chem. Int. Ed. 44, 4554–4557.
Golichenari, B., Nosrati, R., Farokhi-Fard, A., Abnous, K., Vaziri, F., Behravan, J., 2018. Biosens. Bioelectron. 17, 319–331.

Hou, T., Xu, N.N., Wang, W.X., Ge, L., Li, F., 2018. Anal. Chem. 90, 9591–9597.
Hu, C.G., Zheng, J.N., Su, X.Y., Wang, J., Wu, W.Z., Hu, S.S., 2013. Anal. Chem. 85, 10612–10619.
Jing, W.W., Jiang, X.R., Zhao, W., Liu, S.X., Cheng, X.J., Sui, G.D., 2014. Anal. Chem. 86, 5815–5821.
Kim, K., Lee, T.H., Santos, E.J.G., Jo, P.S., Salleo, A., Nishi, Y., Bao, Z.N., 2015. ACS Nano 9, 5922–5928.
Kong, Q.K., Cui, K., Zhang, L.N., Wang, Y.H., Sun, J.L., Ge, S.G., Zhang, Y., Yu, J.H., 2018. Anal. Chem. 90, 11297–11304.
Li, F., Yu, Y.Q., Li, Q., Zhou, M., Cui, H., 2014. Anal. Chem. 86, 1608–1613.
Li, M.J., Liang, W.B., Y, R., C, Y.Q., 2019. ACS Appl. Mater. Interfaces 11, 11834–11840.
Li, M.J., Xiong, C., Zheng, Y.N., Liang, W.B., Yuan, R., Chai, Y.Q., 2018. Anal. Chem. 90, 8211–8216.
Li, M.J., Zheng, Y.N., Liang, W.B., Yuan, R., Chai, Y.Q., 2017. ACS Appl. Mater. Interfaces 9, 42111–42120.
Li, M.J., Zheng, Y.N., Liang, W.B., Yuan, Y.L., Chai, Y.Q., Yuan, R., 2016. Chem. Commun. 52, 8138–8141.
Lian, Z.C., Xu, P.P., Wang, W.C., Zhang, D.Q., Xiao, S.N., Li, X., Li, G.S., 2015. ACS Appl. Mater. Interfaces 7, 4533–4540.
Mi, X.W., He, F.J., Xiang, M.,Y., Lian, Y., Yi, S.L., 2012. Anal. Chem. 84, 939–946.
Schafer, P., van de Linde, S., Lehmann, J., Sauer, M., Doose, S., 2013. Anal. Chem. 85, 3393–3400.
Sypabekova, M., Jolly, P., Estrela, P., Kanayeva, D., 2019. Biosens. Bioelectron. 123, 141–151.
Teengam, P., Siangproh, W., Tuantranont, A., Vilaivan, T., Chailapakul, O., Henry, C.S., 2017. Anal. Chem. 89, 5428–5435.
Wang, H.H., Li, M.J., Zheng, Y.N., Hu, T., Chai, Y.Q., Yuan, R., 2018a. Biosens. Bioelectron. 120, 71–76.
Wang, H.H., Li, M.J., Wang, H.J., Chai, Y.Q., Yuan, R., 2019. ACS Appl. Mater. Interfaces 11, 23765–23772.
Wang, P.P., Sun, G.Q., Ge, L., Ge, S.G., Song, X.R., Yan, M., Yu, J.H., 2013. Chem. Commun. 49, 10400–10402.
Wang, Q., Ruan, Y.F., Zhao, W.W., Lin, P., Xu, J.J., Chen, H.Y., 2018b. Anal. Chem. 90, 3759–3765.
Wu, S., Song, H.L., Song, J., He, C., Ni, J., Zhao, Y.Q., Wang, X.Y., 2014. Anal. Chem. 86, 5922–5928.
Xie, S.B., Dong, Y.W., Yuan, Y.L., Chai, Y.Q., Yuan, R., 2016. Anal. Chem. 88, 5218–5224.
Yan, Z.Y., Wang, Z.H., Miao, Z., Liu, Y., 2016. Anal. Chem. 88, 922–929.
Zhang, N., Ruan, Y.F., Zhang, L.B., Zhao, W.W., Xu, J.J., Chen, H.Y., 2018. Anal. Chem. 90, 2341–2347.
Zhao, M., Fan, G.C., Chen, J.J., Shi, J.J., Zhu, J.J., 2015. Anal. Chem. 87, 12340–12347.
Zhao, W.W., Xu, J.J., Chen, H.Y., 2014. Chem. Rev. 114, 7421–7441.
Zhao, W.W., Xu, J.J., Chen, H.Y., 2018. Anal. Chem. 90, 615–627.
Zhou, J., Lai, W.Q., Zhuang, J.Y., Tang, J., Tang, D.P., 2013. ACS Appl. Mater. Interfaces 5, 2773–2781.